Journal of Catalysis 295 (2012) 59–69

Contents lists available at SciVerse ScienceDirect

Journal of Catalysis

journal homepage: www.elsevier.com/locate/jcat

Adsorbate interactions on surface lead to a flattened Sabatier volcano plot in reduction of oxygen

Liang Qi [a], Ju Li [a,b,*]

[a] Department of Nuclear Science and Engineering, Massachusetts Institute of Technology, Cambridge, MA 02139, USA
[b] Department of Materials Science and Engineering, Massachusetts Institute of Technology, Cambridge, MA 02139, USA

A R T I C L E   I N F O

Article history:
Received 19 October 2011
Revised 18 July 2012
Accepted 19 July 2012
Available online 24 August 2012

Keywords:
Surface Catalysis
Sabatier principle
Volcano Plot
Oxygen Reduction
Adsorbate interactions
Microkinetic model
First-principles calculations
Sensitivity

A B S T R A C T

Ab initio electronic-structure calculations of surface catalysis often give changes ⩾0.1 eV for activation energies of intermediate steps when the surface structure or composition is varied, yet ⩾50-fold change in activity according to naive interpretation of the Arrhenius formula is usually not seen in corresponding experiments. To quantitatively analyze this sensitivity inconsistency between simulations and experiments, we propose a mean-field microkinetic model of electrochemical oxygen reduction reaction on Pt (1 1 1) and (1 0 0) surfaces, which outputs similar steady-state reaction rates despite of large differences in adsorption energies of reaction intermediates and activation energies. Sensitivity analyses indicate lateral repulsions between surface adsorbates ("enthalpic effect") and site competition ("entropic effect") flatten the catalytic activity vs. adsorption strength volcano plot and reduce sensitivity to material elementary energetics, in agreement with the observed experimental sensitivity behavior. Our analyses provide a systematic method to quantitatively investigate sensitivities of surface reactions when the mean-field approximation is reasonable.

1. Introduction

Quantum mechanical electronicstructure interactions between adsorbates and catalytic surfaces are critical parameters to control the activity of catalytic reactions. Qualitatively, Sabatier principle suggests that the most active catalyst should have moderate adsorption strength [1]. If the interactions are too weak, the reactants would be difficult to bind to the catalyst and few reactions take place; on the other hand, if the interactions are too strong, the catalyst would be blocked by reaction intermediates or products that impede further reactions. Quantitatively, the relation between catalytic activity and adsorption energy for certain reactant/intermediate E_{ADS} is obtained based on microkinetic model [2]. A simplified picture is that reaction rate r can be described by Arrhenius relation $r = \upsilon \times \exp\left(-\frac{Q_A^{\mathrm{RDS}}}{k_B T}\right)$, where Q_A^{RDS} is the activation free energy of rate-determining step (RDS). Changes of Q_A^{RDS} on different surfaces are assumed to be linearly related to variations of E_{ADS} according to thermal-kinetic models (such as $\delta Q_A^{\mathrm{RDS}} \approx \pm\delta E_{\mathrm{ADS}}$) [2–4]. As shown by the dashed lines in Fig. 1, the crossing of two $Q_A^{\mathrm{RDS}}(E_{\mathrm{ADS}})$ linear functions that correspond to the weak and strong adsorption situations, respectively, leads to a "volcano plot". It not only predicts the catalytic activity variations on different surfaces based on first-principles calculations, but also gives the possible maximum activity and the corresponding optimal adsorption strength $E_{\mathrm{ADS}}^{\mathrm{OPT}}$.

However, this volcano plot based on naive interpretation of Arrhenius relation results in a question on the consistency between theoretical studies and experimental measurements for the sensitivity of reaction rate to adsorption strengths on different catalytic materials. First-principles calculations of surface catalysis often give changes in E_{ADS} with magnitude of 0.1–0.5 eV when the surface structure or composition is varied a little bit, such as from Pt (1 1 1) to Pt alloy (1 1 1) with pure Pt top layer, yet significant change according to the Arrhenius expression in catalytic activity at room temperature $\left(\exp\left(-\frac{0.1\ \mathrm{eV}}{k_B \cdot 300\ \mathrm{K}}\right) \approx 50\right)$ is usually not seen experimentally, for example, despite decades of experimental efforts to increase the catalytic activity of Pt-based alloys for electrochemical oxygen reduction reaction (ORR), only small enhancements (no more than 10 times of specific activity) have been achieved and most of Pt alloys have similar specific activity [5–8]. Even for pure Pt, with large differences in E_{ADS} (~0.5 eV), Pt (1 1 1), (1 1 0), and (1 0 0) surfaces were still found to have comparable ORR specific activities [6]. Recently, Strasser et al. tuned adsorption strength of Pt surface by lattice strain and found that the rate variations do not change like the volcano plot prediction

* Corresponding author at: Department of Materials Science and Engineering, Massachusetts Institute of Technology, Cambridge, MA 02139, USA.
E-mail address: liju@mit.edu (J. Li).

0021-9517/$ - see front matter © 2012 Elsevier Inc. All rights reserved.
http://dx.doi.org/10.1016/j.jcat.2012.07.019

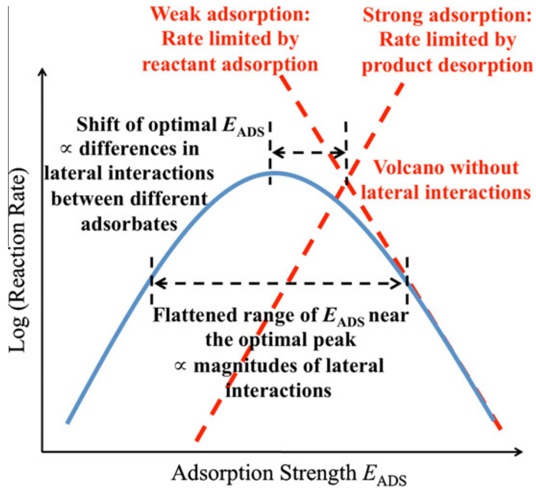

Fig. 1. Relation between catalytic activity and adsorption strength for certain surface reaction, so-called "volcano plot". Dashed lines are based on simple Arrhenius relation; solid line is obtained with the consideration of lateral interactions between adsorbed reaction intermediates.

in the region close to the optimal: log (Reaction rate)(E_{ADS}) should behave as a flat top instead of a sharp summit according to Arrhenius relation as the dashed line crossing in Fig. 1 [4,9], and its predicted highest possible activity at optimal E_{ADS} is not achieved.

To resolve these inconsistencies in both sensitivity and maximum activity, kinetic model beyond simple Arrhenius relation should be applied to investigate the overall performance of catalytic reaction network [2,10,11]. Several studies suggested that there could be multiple RDS, and the competitions between them for limited reaction sites or surface adsorbates could lower the sensitivities [2,10,12–14]. Since these competitions are the physical origins of configurational entropies of surface adsorbates, they can be named as "entropic effects". Meanwhile, some microkinetic models indicated the necessity to consider interactions between surface adsorbates [5,10,15–20], which can be named as "enthalpic effects" since they change the energy/enthalpy of individual adsorbate. These effects are usually very strong for large atoms/molecules, where the change of adsorption energy for individual adsorbate can be on the order of 1 eV when the coverage is more than 0.5 monolayer (ML) [21]. To systematically analyze these two types of effects and build accurate connections between atomic energetics from theoretical calculations and macroscopic reaction kinetics, we propose a mean-field microkinetic model based on first-principles calculations to simulate ORR on Pt (111) and (100) surfaces, which considers both entropic and enthalpic interactions between surface adsorbates. We also apply *sensitivity analysis* to this model, which can quantitatively indicate how each energetic parameter, such as the energy/enthalpy for a specific reaction intermediate or transition state, can affect the overall output of reaction network [22–24]. A robust result of the microkinetic model is the low sensitivity of ORR rate to materials energetics, and our analyses indicate most of it originates not from entropic effects, but from enthalpic effects under strong enthalpic interactions obtained from density functional theory (DFT) calculations, which is similar with the conclusion of another microkinetic model on CO oxidation [19]. These enthalpic interactions result in significantly flattened Sabatier volcano plot and the shift of E_{ADS}^{OPT}, as illustrated by the solid curve in Fig. 1. However, the quantitative agreement between this volcano plot and the experimental results depends on accuracy of surface reaction model and mean-field approximation, which will be discussed later in this paper.

The paper is organized as following: In Section 2, we explain the mean-field microkinetic ORR model, the methodologies to obtain model parameters for Pt (111)/(100) surfaces, and the formula of sensitivity analysis. In Section 3, we numerically solve this model on these two surfaces and investigate the corresponding kinetics at different electrode potential U. In Section 4, we analyze the sensitivities of ORR rate to individual energetic parameters on Pt (111) and (100) surfaces, investigate the effects of enthalpic interactions between surface adsorbates on the sensitivities and Sabatier volcano, and compare the theoretical volcano plot with its experimental counterpart. The conclusions are summarized in Section 5.

2. Methods

2.1. Microkinetic model

ORR on the cathode of proton-exchange-membrane (PEM) fuel cells is a multi-electron transfer reaction. Its electron transfer mechanism depends on the charge states of ORR intermediates adsorbed on catalytic surface. For example, the charge state of adsorbed O_2 (O_2^*, where $*$ means adsorbed state or empty surface site), determines the electron transfer process in oxygen adsorption ($O_2 + * \rightarrow O_2^*$ or $O_2 + * + e^- \rightarrow O_2^{-*}$). We found that these intermediates, such as O_2^*, are in near-neutral states [25], so the transfers of 4 electrons for each O_2 occur concurrently with 4 proton transferred from the acidic electrolyte, that is, all electron transfers are proton-coupled (PCET) [26]. Based on PCET mechanism, we consider the following elementary reactions in our model:

Step 1: Molecular Adsorption (**MA**): $O_2 + * \rightarrow O_2^*$.
Step 2a: Direct Dissociation (**DD**): $O_2^* + * \rightarrow O^* + O^*$.
Step 2b: Associated Dissociation (**AD**): $O_2^* + * + H^+ + e^- \rightarrow O^* + OH^*$.
Step 3: Oxygen Protonation (**OP**): $O^* + H^+ + e^- \rightarrow OH^*$.
Step 4: Hydroxyl Protonation (**HP**): $OH^* + H^+ + e^- \rightarrow H_2O + *$.

Similar reaction steps were applied in previous ORR microkinetic models [3,12,13]. Here, we omit other possible intermediates, such as OOH^* and $H_2O_2^*$ [27,28], because OOH^* on Pt surface may have low energy barrier to dissociate into O^* and OH^*(0.22 eV) [29], and H_2O_2 formation on Pt surface is significant only when electrode potential is much lower (<0.3 V vs. Standard Hydrogen Electrode (SHE) [27]. In this paper, all the potential values are relative to SHE.) than the normal cathode potential region (0.6–1.0 V). The reaction rate for each step r_i is expressed like the following:

$$r_{MA} = k_{MA}^+ \theta_* - k_{MA}^- \theta_{O_2^*} \quad (1)$$

$$r_{DD} = k_{DD}^+ \theta_{O_2^*} \theta_* - k_{DD}^- \theta_{O^*}^2 \quad (2)$$

$$r_{AD} = k_{AD}^+ \theta_{O_2^*} \theta_* - k_{AD}^- \theta_{O^*} \theta_{OH^*} \quad (3)$$

$$r_{OP} = k_{OP}^+ \theta_{O^*} - k_{OP}^- \theta_{OH^*} \quad (4)$$

$$r_{HP} = k_{HP}^+ \theta_{OH^*} - k_{HP}^- \theta_* \quad (5)$$

where $\theta_{O_2^*}, \theta_{O^*}, \theta_{OH^*}$ and θ_* is the coverage of O_2^*, O^*, OH^* and empty sites on the surface, respectively, and $\theta_* = (1ML - \theta_{O_2^*} - \theta_{O^*} - \theta_{OH^*})$. The rate constants of forward and reverse reactions for each step are:

$$k_i^+ = \upsilon_i^+ \exp\left(-\frac{Q_i^+}{k_B T}\right),$$

$$k_i^- = \upsilon_i^- \exp\left(-\frac{Q_i^-}{k_B T}\right) = \upsilon_i^- \exp\left(-\frac{\max(0, Q_i^+ - \delta G_i)}{k_B T}\right) \quad (6)$$

where $\upsilon_i^+/\upsilon_i^-$ is the pre-exponential constant of the forward/reverse reaction at a single reaction site for step i; Q_i^+/Q_i^- is activation free energy of the forward/reverse reaction; δG_i is the reaction free energy at individual reaction site without configurational entropy, which would be automatically included into the reaction network through θ_i^* in the pre-exponential factors of each reaction rate equation (Eqs. (1)–(5)). At steady states, $\theta_{O_2^*}$, θ_{O^*} and θ_{OH^*} do not change, so the steady-state reaction rate for each step can be obtained by solving the following equation numerically

$$\begin{bmatrix} \frac{d\theta_{O_2^*}}{dt} \\ \frac{d\theta_{O^*}}{dt} \\ \frac{d\theta_{OH^*}}{dt} \end{bmatrix} = \begin{bmatrix} 1 & -1 & -1 & 0 & 0 \\ 0 & 2 & 1 & -1 & 0 \\ 0 & 0 & 1 & 1 & -1 \end{bmatrix} \begin{bmatrix} r_{MA} \\ r_{DD} \\ r_{AD} \\ r_{OP} \\ r_{HP} \end{bmatrix} = [\mathrm{A}][\vec{r}_{\mathrm{I}}] = \begin{bmatrix} 0 \\ 0 \\ 0 \end{bmatrix} \tag{7}$$

Here matrix [A] describes the effect of reaction network on ORR intermediates, and vector $[\vec{r}_{\mathrm{I}}]$ is reaction rate of each step (Eqs. (1)–(5)). The total current density of ORR at steady state is calculated as the following

$$\begin{aligned} j_k &= [0 \quad 0 \quad 1 \quad 1 \quad 1] \cdot [r_{MA} \quad r_{DD} \quad r_{AD} \quad r_{OP} \quad r_{HP}]^{\mathrm{T}} \times e/S_0 \\ &= [\vec{\mathrm{B}}]^{\mathrm{T}} \cdot [\vec{r}_{\mathrm{I}}] \times e/S_0 \end{aligned} \tag{8}$$

because electron transfer only occurs in three steps (**AD**, **OP**, and **HP**). Here, vector $[\vec{\mathrm{B}}]$ describes the effect of reaction network on final reaction product; S_0 is the surface area of one reaction site; and j_k is *kinetic current density*, which is determined only by the surface reaction kinetics other than mass transfer effects.

2.2. Model of energetic parameters

To solve the above reaction network, the energetic parameters, $Q_i^+/\delta G_i$, and the pre-exponential factors, $\upsilon_i^+/\upsilon_i^-$, should be obtained explicitly for each elementary reaction step as Eq. (6). These parameters can be calculated by theoretical methods based on certain dynamic model at electronic/atomic scales, which are described as the following.

2.2.1. Proton-coupled electron transfer

Three elementary reactions (**AD**, **OP**, and **HP**) can be considered as PCET. As shown in Fig. 2, PCET is completed by two sequential steps: proton transfer from the electrolyte far away from the electrode to the area close to electrode surface, and proton transfer from the electrolyte near the surface to ORR intermediate adsorbed on the surface, where proton meets the electron transferred from the electrode.

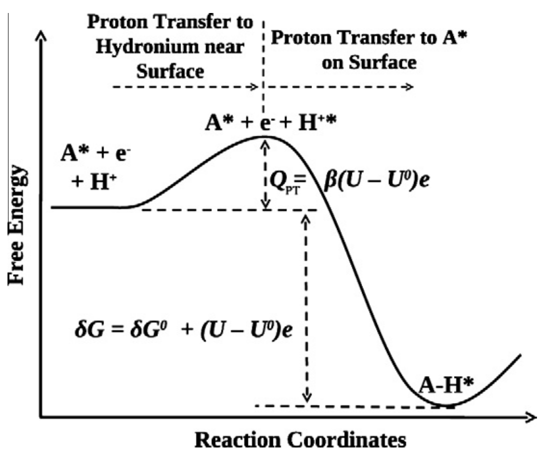

Fig. 2. Reaction path of proton-coupled electron transfer (PCET) $A^* + H^+ + e^- \rightarrow AH^*$. Here, H^{+*} is the proton in the hydronium $H^+(H_2O)_n$ near the electrode surface.

Protons in bulk electrolyte always exist in the hydrated forms, so-called "hydronium" $H^+(H_2O)_n$ [30–32]. It would require excess energy to transfer a proton from hydronium in the bulk electrolyte to hydronium near the surface, because a proton has different free energies at two different conditions (bulk vs. surface) resulting from the changes in solvation shell and/or electric field applied on the proton/hydronium [33]. This excess energy would increase as the electrode potential U increases, since more positive U results from more positive excess charges on the electrode surface, which would increase the repulsive energy between hydronium and electrode. Here, we simply assume the activation free energy of this bulk-to-surface transfer process, Q_{PT}, changes linearly with U as following

$$Q_{PT} = \beta(U - U^0)e \tag{9}$$

where U^0 is the electrode potential at which $Q_{PT} = 0$, and β is the linear coefficient.

In the second step, the proton on the hydronium near the surface would transfer to ORR intermediate adsorbed on the surface. Similar with the proton transfer in the bulk water [32], DFT calculations suggested that this could be a low-barrier (<0.1 eV) process as long as it is an exothermic reaction [29]. On the other hand, the reaction energy depends on the stabilities of adsorbed intermediates and electrode potential, so this step could also be an endothermic reaction. Under this condition, it is a reasonable assumption to use the positive reaction free energy δG_i as an approximate value of the activation free energy [3]. Combining two steps together, we can assume Q_i^+ of a whole PCET step at different electrode potential U as

$$\begin{aligned} Q_i^+ &= Q_{PT} = \beta(U - U^0)e \quad \text{if} \quad \delta G_i < Q_{PT} \\ &= \delta G_i = \delta G_i^0 + (U - U^0)e \quad \text{otherwise} \end{aligned} \tag{10}$$

δG_i is a function of electrode potential U, which only changes the chemical potential of the electrons [34], and chemical potential of adsorbates as reaction intermediates. When U is low, δG_i is always negative so that Q_{PT} is dominant. Thus, U^0 can be regarded as electrode potential when $Q_i^+ = 0$. In experimental measurements of ORR polarization curves at low U region ($\lesssim 0.8$ V) on Pt surfaces, the overall reaction activation energy is approximately $0.5 \times (U - 0.3\text{ V})$ eV [35], so we can set $U^0 = 0.3$ V and $\beta = \frac{1}{2}$. Here, β can be regarded as the well-defined *transfer coefficient* on how the activation free energy changes with the reaction free energy. So Eq. (10) can automatically describe the transition of β from $\beta \approx \frac{1}{2}$ to $\beta \approx 1$ as U increases observed in experimental "Tafel plots" [36]. This U-dependent character of β was also found in other theoretical calculations [37–39].

To obtain δG_i of PCET steps, we use the reaction free energy of hydrogen oxidation reaction (HOR) $H_2 \rightarrow 2H^+ + 2e^-$ at standard conditions ($T = 300$ K, pH = 0, $p_{H_2} = 1$ atm, $p_{H_2O} = 0.035$ atm because it is the equilibrium pressure of liquid H_2O at 300 K) [3], which is $\delta G = 2e \cdot U$. Thus, the reaction free energy for step **AD**, **OP**, and **HP** can be written as the following

$$\delta G_{AD} = \mu_{O^*} + \mu_{OH^*} - \mu_{O_2^*} - \frac{1}{2}\mu_{H_2}^0 + e \cdot U \tag{11}$$

$$\delta G_{OP} = \mu_{OH^*} - \mu_{O^*} - \frac{1}{2}\mu_{H_2}^0 + e \cdot U \tag{12}$$

$$\delta G_{HP} = \mu_{H_2O}^0 - \mu_{OH^*} - \frac{1}{2}\mu_{H_2}^0 + e \cdot U \tag{13}$$

where $\mu_{O_2^*}$, μ_{O^*} and μ_{OH^*} are the chemical potentials of O_2^*, O^* and OH^* at individual reaction site without configurational entropy; $\mu_{H_2O}^0$ and $\mu_{H_2}^0$ is chemical potential of H_2O and H_2, respectively, at standard conditions. $\mu_{O_2^*}$, μ_{O^*}, and μ_{OH^*} depend on the detailed reaction environment such as surface adsorbate coverage because of enthalpic lateral interactions between these adsorbates

[10,15,5,16–20]. Here, we use mean-field linear approximations to express these chemical potentials as

$$\begin{bmatrix} \mu_{O_2^*} \\ \mu_{O^*} \\ \mu_{OH^*} \end{bmatrix} \approx \begin{bmatrix} h^0_{O_2^*} \\ h^0_{O^*} \\ h^0_{OH^*} \end{bmatrix} + \begin{bmatrix} \zeta^{O_2^*}_{O_2^*} & \zeta^{O^*}_{O_2^*} & \zeta^{OH^*}_{O_2^*} \\ \zeta^{O_2^*}_{O^*} & \zeta^{O^*}_{O^*} & \zeta^{OH^*}_{O^*} \\ \zeta^{O_2^*}_{OH^*} & \zeta^{O^*}_{OH^*} & \zeta^{OH^*}_{OH^*} \end{bmatrix} \begin{bmatrix} \theta_{O_2^*} \\ \theta_{O^*} \\ \theta_{OH^*} \end{bmatrix} \tag{14}$$

where $h^0_{i^*}$ is the enthalpy for surface adsorbate i^* on clean surface. $h^0_{i^*}$ can be obtained from DFT calculations by the following equation:

$$h^0_{i^*} = E_{\text{surface}+i^*} + \text{ZPE}_{i^*} - E_{\text{surface}} \tag{15}$$

where $E_{\text{surface}+i^*}$ and E_{surface} is the ground-state energy of surface with adsorbate i^* and clean surface itself, respectively; ZPE_{i^*} is the zero point energy from the vibration modes of i^*. $\zeta^{j^*}_{i^*}$ is the linear dependence coefficient of μ_{i^*} on θ_{j^*}. $\zeta^{j^*}_{i^*}$ can also be considered as the second order partial derivatives of Gibbs free energy of total system, G_{tot}, to θ_{i^*} and θ_{j^*} ($\zeta^{j^*}_{i^*} = \frac{1}{N^2_{\text{site}}} \cdot \frac{\partial^2 G_{\text{tot}}}{\partial\theta_{i^*}\partial\theta_{j^*}}$), thus $\zeta^{j^*}_{i^*} = \zeta^{i^*}_{j^*}$ and there are only six independent $\zeta^{j^*}_{i^*}$ parameters.

2.2.2. Oxygen adsorption and dissociation

For the step **MA**. we assume its activation barrier Q^+_{MA} equals zero if the adsorption energy of O_2 molecule $E^{O_2^*}_{\text{ads}} < 0$, where E stands for the ground-state energy and $E^{O_2^*}_{\text{ads}} \equiv E_{\text{surface}+O_2^*} - (E_{\text{surface}} + E_{O_2})$, otherwise $Q^+_{\text{MA}} = E^{O_2^*}_{\text{ads}}$. For the pre-exponential factors, we can set $\upsilon^-_{\text{MA}} \sim 10^{13}\ \text{s}^{-1}\ \text{site}^{-1}$ for its reverse step, comparable with the vibrational frequencies of the adsorbates [40]. However, it is a much more complex and multi-scale problem to determine the pre-exponential factor for oxygen adsorption υ^+_{MA}, because mass transport of O_2 on the cathode of PEM fuel cell depends not only on O_2 partial pressure p_{O_2}, but also many other factors like the O_2 convection in cathode gas channel and O_2 diffusion in the gas diffusion layer (GDL) [41–43]. To simplify this problem, we set υ_{MA} as pre-exponential factor for typical surface reactions controlled by molecular adsorption, $5 \times 10^4\ \text{s}^{-1}\ \text{site}^{-1}$ [1,44]. Under this value, the diffusion limiting current density from our model is ~30 A/cm^2 indicated by the plateau of current density at low potential region as shown in Fig. 3, which is comparable with the limiting current density of real PEM fuel cell (1–10 A/cm^2) [45]. Thus, we set

$$k^+_{\text{MA}} = 5 \times 10^4 \exp\left[-\frac{\max\left(0, E^{O_2^*}_{\text{ads}}\right)}{k_B T}\right] (\text{s}^{-1}\ \text{site}^{-1})$$

$$k^-_{\text{MA}} = 10^{13} \exp\left[-\frac{\max\left(0, -E^{O_2^*}_{\text{ads}}\right)}{k_B T}\right] (\text{s}^{-1}\ \text{site}^{-1}) \tag{16}$$

For step **DD**, the pre-exponential factor can also be approximated by adsorbate vibrational frequencies, and we write the reaction constants of step **DD** as

$$k^+_{\text{DD}} = 10^{13} \exp\left(-\frac{E^{\text{DD}}_a}{k_B T}\right) (\text{s}^{-1}\ \text{site}^{-1})$$

$$k^-_{\text{DD}} = 10^{13} \exp\left(-\frac{E^{\text{DD}}_a + E^{O_2^*}_{\text{ads}} - 2 \cdot E^{O^*}_{\text{ads}}}{k_B T}\right) (\text{s}^{-1}\ \text{site}^{-1}) \tag{17}$$

where E^{DD}_a is the activation energy of O_2^* dissociation and $E^{O^*}_{\text{ads}}$ is the adsorption energy of atomic oxygen O* defined as $E^{O^*}_{\text{ads}} \equiv E_{\text{surface}+O^*} - (E_{\text{surface}} + \frac{1}{2}E_{O_2})$. All these energetic parameters ($E^{O_2^*}_{\text{ads}}, E^{O^*}_{\text{ads}}$, and E^{DD}_a) may change when the surface is covered by many adsorbates with significant lateral interactions. Similarly with PCET steps as Eq. (14), the adsorbate coverage effects to $E^{O_2^*}_{\text{ads}}, E^{O^*}_{\text{ads}}$, and E^{DD}_a can be written as the following:

$$\begin{bmatrix} E^{O_2^*}_{\text{ads}} \\ E^{O^*}_{\text{ads}} \\ E^{\text{DD}}_a \end{bmatrix} \approx \begin{bmatrix} E^{O_2^*}_{\text{ads0}} \\ E^{O^*}_{\text{ads0}} \\ E^{\text{DD}}_{a0} \end{bmatrix} + \begin{bmatrix} \zeta^{O_2^*}_{O_2^*} & \zeta^{O^*}_{O_2^*} & \zeta^{OH^*}_{O_2^*} \\ \zeta^{O_2^*}_{O^*} & \zeta^{O^*}_{O^*} & \zeta^{OH^*}_{O^*} \\ \zeta^{O_2^*}_{DD^*} & \zeta^{O^*}_{DD^*} & \zeta^{OH^*}_{DD^*} \end{bmatrix} \begin{bmatrix} \theta_{O_2^*} \\ \theta_{O^*} \\ \theta_{OH^*} \end{bmatrix} \tag{18}$$

where $E^{O_2^*}_{\text{ads0}}, E^{O^*}_{\text{ads0}}$, and E^{DD}_{a0} are values on clean surface.

2.2.3. Parameters on Pt (111) and (100) Surfaces

For summary, there are 15 energetic parameters in the microkinetic model for a specific surface: 9 from Eq. (14) (3 $h^0_{i^*}$ and 6 $\zeta^{j^*}_{i^*}$) and 6 from Eq. (18) ($E^{O_2^*}_{\text{ads0}}, E^{O^*}_{\text{ads0}}, E^{\text{DD}}_{a0}$, $\zeta^{O_2^*}_{\text{DD}}, \zeta^{O^*}_{\text{DD}}$ and $\zeta^{OH^*}_{\text{DD}}$). Here, $E^{O_2^*}_{\text{ads0}}/E^{O^*}_{\text{ads0}}$ is related to $h^0_{O_2^*}/h^0_{O^*}$ and the corresponding ZPE as Eq. (15). All these energetic parameters can be calculated from DFT methods. We apply such DFT calculations to Pt (111) and (100) surfaces, which are two typical low-index facets for Pt crystal. The calculations are performed by using the Vienna Ab-Initio Simulation Package (VASP) [46,47] with projector augmented wave (PAW) potentials [48] and Perdew–Burke–Ernzerhof (PBE) exchange–correlation functional [49]. To obtain $\zeta^{i^*}_{i^*}$ for adsorbate i^*,

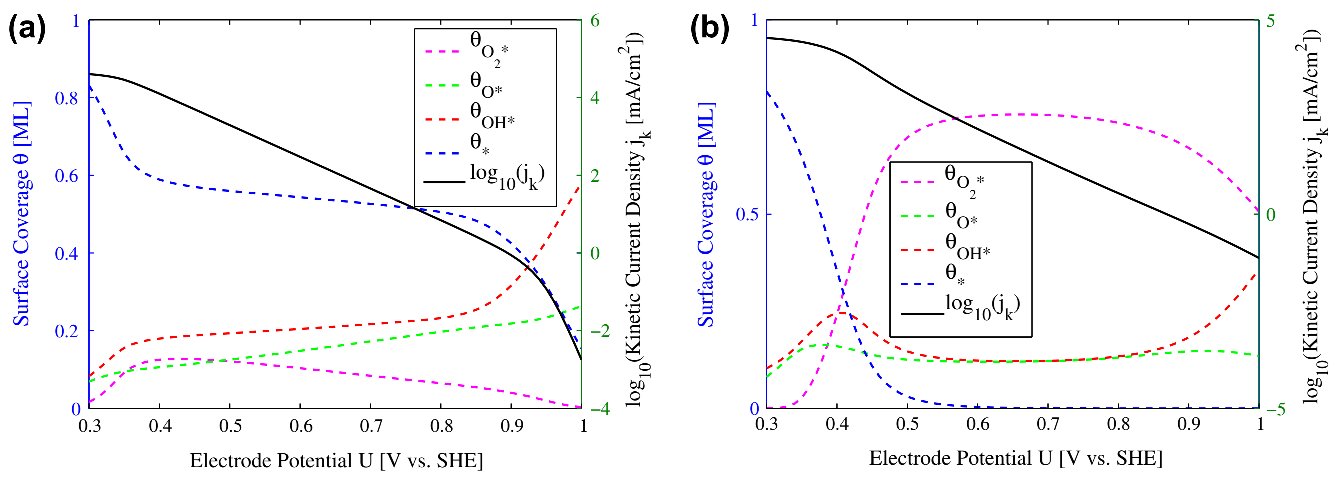

Fig. 3. Surface coverage of ORR intermediates (dashed curves with *y*-axis label on the left) and kinetic current density j_k (solid curves with *y*-axis label on the right) vs. electrode potential *U* on Pt (111) (a) and (100) (b) surface at steady states.

Table 1
Energetic parameters of adsorbates on Pt (1 1 1) and Pt (1 0 0) surfaces. All data are in unit of eV. ZPEs are obtained on Pt (1 1 1) surface by DFT calculations.

	$E_{ads0}^{O_2^*}$	$E_{ads0}^{O^*}$	$h_{O_2^*}^0$	$h_{O^*}^0$	$h_{OH^*}^0$	E_{a0}^{DD}
Pt (1 1 1)	−0.655	−1.184	−10.359	−6.034	−9.941	0.27
Pt (1 0 0)	−1.115	−1.141	−10.819	−5.992	−10.527	0.16

Table 2
Parameters of lateral interaction strengths $\zeta_{i^*}^{j^*}$ on Pt (1 1 1) and Pt (1 0 0) surfaces. All data are in unit of eV/ML.

	$\zeta_{O_2^*}^{O_2^*}$	$\zeta_{O^*}^{O^*}$	$\zeta_{OH^*}^{OH^*}$	$\zeta_{O_2^*}^{O^*}$	$\zeta_{O_2^*}^{OH^*}$	$\zeta_{O^*}^{OH^*}$	$\zeta_{DD^*}^{O_2^*}$	$\zeta_{DD}^{O^*}$	$\zeta_{DD}^{OH^*}$
Pt (1 1 1)	0.71	2.06	0.12	0.71	0.12	0.12	0.36	1.71	0.06
Pt (1 0 0)	0.38	1.28	0.63	0.38	0.38	0.63	0.19	1.09	0.44

a series of DFT calculations are performed, where i^* is consecutively deposited on (1 1 1)/(1 0 0) surface from 0 ML to high coverage close to 1 ML. More details are in Supplementary materials.

The results of all 15 energetic parameters for Pt (1 1 1) and (1 0 0) surfaces are summarized in Tables 1 and 2. Meanwhile, the area of each reaction site S_0 is set as 6.654 Å^2 and 7.683 Å^2 for Pt (1 1 1) and (1 0 0) surface, respectively, and temperature $T = 300$ K. There are also two surface-independent parameters, $\mu_{H_2}^0$ and $\mu_{H_2O}^0$, and our DFT calculations plus the thermodynamic corrections give the results as $\mu_{H_2}^0 = -6.796$ eV, and $\mu_{H_2O}^0 = -14.203$eV.

Using the parameters obtained on Pt (1 1 1) and Pt (1 0 0) surfaces, we can solve Eqs. (7) and (8) to obtain j_k at steady states. However, there are still remaining uncertainties, the pre-exponential factors $\upsilon^{+/-}$ for three PCET steps (**AD**, **OP** and **HP**). Here, we assume all these pre-exponential factors are equal, designated as υ_H (pH dependent). It is found that if we set $\upsilon_H = 1 \times 10^6$ (s^{-1} site^{-1}), $j_k = 0.88$ mA cm^{-2} on Pt (1 1 1) surface when $U = 0.9$ V, comparable with experimental results [7,50,51]. In fact, υ_H on the order of 10^6 (s^{-1} site^{-1}) can also be obtained from the multiplication of S_0 and proton diffusion flux near the surface, which can be estimated by proton diffusion coefficient in water ($\sim 10^{-9}$ m^2/s [52]) multiplied by proton concentration (~1 mol/L at pH = 0) then divided by the typical Debye length in electrolyte (~10 nm [53]).

2.3. Methods for sensitivity analysis

As the discussions in the introduction, we intend to investigate how the overall reaction rate changes with the surface adsorption strength. The best method to quantitatively study it is to apply the sensitivity analysis [22–24]. Thus, sensitivity is calculated when only one energetic parameter, such as enthalpy $h_{i^*}^0$ for adsorbate i^* on clean surface, is changed, but all other energetic parameters are fixed. This first-order sensitivity $\frac{d\ \log_{10}(j_k)}{d\ h_{i^*}^0}$ can be calculated analytically based on Eq. (8) as the following:

$$\frac{d\log_{10}(j_k)}{dh_{i^*}^0} = \frac{e}{\log(10) \cdot j_k S_0} \cdot [\vec{B}]^T \cdot \left\{ \left[\frac{\partial \vec{r}_I}{\partial h_{i^*}^0}\right] + \left[\frac{\partial \vec{r}_I}{\partial \theta_{j^*}}\right] \cdot \left[\frac{d\theta_{j^*}}{dh_{i^*}^0}\right] \right\} \tag{19}$$

where the elements in vector $\left[\frac{\partial \vec{r}_I}{\partial h_{i^*}^0}\right]$ and matrix $\left[\frac{\partial \vec{r}_I}{\partial \theta_{j^*}}\right]$ are partial derivatives of each elementary step's rate with respect to $h_{i^*}^0$ and θ_{j^*}, respectively. All of them can be directly calculated because all rate equations from Eqs. (1)–(5) have analytic expressions from reaction dynamics models in Section 2.2. On the other hand, the elements in vector $\left[\frac{d\theta_{j^*}}{dh_{i^*}^0}\right]$ are the total derivatives of θ_{j^*} with respect to $h_{i^*}^0$, which cannot be calculated directly. However, because the constraints of steady states by Eq. (7) ($[A][\vec{r}_I] = 0$), we can obtain the following relation

$$\left[\frac{d\ ([A][\vec{r}_I])}{dh_{i^*}^0}\right] = [A]\left[\frac{d\vec{r}_I}{dh_{i^*}^0}\right] = [A]\left\{ \left[\frac{\partial \vec{r}_I}{\partial h_{i^*}^0}\right] + \left[\frac{\partial \vec{r}_I}{\partial \theta_{j^*}}\right] \cdot \left[\frac{d\theta_{j^*}}{dh_{i^*}^0}\right] \right\} = 0 \tag{20}$$

Then, $\left[\frac{d\theta_{j^*}}{dh_{i^*}^0}\right]$ can be written as a function of $\left[\frac{\partial \vec{r}_I}{\partial h_{i^*}^0}\right]$ and $\left[\frac{\partial \vec{r}_I}{\partial \theta_{j^*}}\right]$ as

$$\left[\frac{d\theta_{j^*}}{dh_{i^*}^0}\right] = -\left[[A]\left[\frac{\partial \vec{r}_I}{\partial \theta_{j^*}}\right]\right]^{-1}[A]\left[\frac{\partial \vec{r}_I}{\partial h_{i^*}^0}\right] \tag{21}$$

So the final results are

$$\frac{d\log_{10}(j_k)}{dh_{i^*}^0} = \frac{e}{\log(10) \cdot j_k S_0} \cdot [\vec{B}]^T \cdot \left(\mathbf{I} - \left[\frac{\partial \vec{r}_I}{\partial \theta_{j^*}}\right]\left[[A]\left[\frac{\partial \vec{r}_I}{\partial \theta_{j^*}}\right]\right]^{-1}[A] \right)\left[\frac{\partial \vec{r}_I}{\partial h_{i^*}^0}\right] \tag{22}$$

where $\mathbf{I}$ is the identity matrix. The sensitivity of ORR rate to the activation energy of step **DD** on clean surface, $\frac{d\ \log_{10}(j_k)}{dE_{a0}^{DD}}$, can be calculated by the same formula as Eq. (22). We should emphasis that Eq. (22) is a general formula for surface reaction network, where [A] and $[\vec{B}]$ describe the effects of surface reaction network to reaction intermediates and final products, respectively. When the system changes to other surface reactions other than ORR, sensitivity analysis based on Eq. (22) is still correct.

3. Results on Pt (1 1 1) and (1 0 0) surfaces

The steady-state solutions $\left(\frac{d\theta_{O_2^*}}{dt} = \frac{d\theta_{O^*}}{dt} = \frac{d\theta_{OH^*}}{dt} = 0\right)$ are calculated when U increases from 0.3 V to 1.0 V vs. SHE with $\upsilon_H = 1 \times 10^6$ (s^{-1} site^{-1}); the results of θ_{i^*} and kinetic current density j_k, which are totally decided by surface kinetics without long-range mass transfer effects, as functions of U on Pt (1 1 1) and (1 0 0) surfaces are shown in Fig. 3a and b, respectively. Here, $\log_{10}(j_k)$ vs. U, so-called "Tafel plot", is presented. Results on both surfaces indicate that there are different potential regions with different ORR kinetics.

As shown in Fig. 3a, at very low U region ($U < 0.37$ V), because there are only negligible activation barriers for proton transfers or surface reactions, j_k is limited by the maximum O_2 adsorption rate ($\upsilon_{MA} = 5 \times 10^4$ (s^{-1} site^{-1}) $\ll \upsilon_H$) and slowly varies with U, meanwhile, ORR intermediates quickly accumulate on the clean surface and the coverage of available surface sites, θ_*, decreases correspondingly. At medium U region (0.37 V < U < 0.85 V), the accumulation slopes of intermediates relative to U become much smaller because of their lateral repulsive interactions; in addition, with a high pre-exponential factor, O_2^* desorption process is more sensitive to these lateral energy changes so that $\theta_{O_2^*}$ decreases gradually to compensate the increases of θ_{O^*} and θ_{OH^*}. As a result, θ_* is almost constant and the barrier to transfer proton from bulk electrolyte to the area near electrode surface, which increases as $\beta(U - U^0)e$ according to Eq. (9), becomes the most dominate factor to determine j_k. Under these conditions, $\log_{10}(j_k)(U)$ behaves as a straight line and Tafel slope can be obtained as $\frac{dU}{d\log_{10}(j_k)} = -\frac{\log(10) \cdot k_B T}{\beta e}$. When $T = 300$ K and $\beta = \frac{1}{2}$, the result is −117 mV/decade, agreeing with experiments [27,35,36].

In high U region ($U > 0.85$ V), ORR kinetics are more complex. As shown in Fig. 3a, the slope of function $\theta_{OH^*}(U)$ increases dramatically because it is thermodynamically favorable to obtain OH* from the reverse reaction of step **HP**, so θ_* decreases significantly with U. Under these conditions, j_k is limited by several factors: the barrier of proton transfer, the positive reaction energies of certain elementary steps, and empty reaction sites available. As a result, j_k decreases more rapidly at high U region and $\left|\frac{dU}{d\log_{10}(j_k)}\right|$ decreases

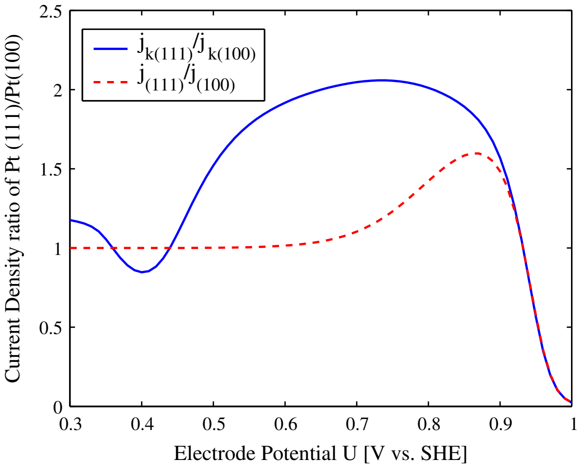

Fig. 4. The ratios of j_k and $j \equiv 1/\left(\frac{1}{j_k}+\frac{1}{j_d}\right)$ between Pt (1 1 1) and Pt (1 0 0) surfaces under the diffusion-limited current density $j_d = 5\ \mathrm{mA\,cm^{-2}}$, comparable with normal experimental procedures [27,36,6,7].

with U gradually from 117 mV/decade to 38 mV/decade when $U > 0.95$ V. Such transition of Tafel slope was also observed in experiments [36], which showed $\frac{dU}{d\log_{10}(j_k)} \approx -77$ mV/decade on Pt (1 1 1) surface when 0.85 V < U < 0.9 V. Too low $\left|\frac{dU}{d\log_{10}(j_k)}\right|$ values at extremely high U region in our microkinetic model may originate from over-occupation of reaction sites by ORR intermediates, where θ_{i^*} is higher than certain critical value so that our simplification of $\mu_{i^*}(\theta_{i^*})$ as linear functions in Eq. (14) is not accurate, which is also illustrated in Fig. 8 of Supplementary materials.

Results of ORR kinetics and reaction pathways on Pt (1 0 0) surface are shown in Fig. 3b. Similar with Pt (1 1 1) surface, the kinetics on (1 0 0) surface can also be classified into different potential regions. At low U region (U < 0.4 V), initially j_k is almost a constant value limited by O_2 adsorption, then ORR intermediates, especially O_2^*, quickly accumulate on the clean surface and the available surface sites decrease significantly, so $\left|\frac{dU}{d\log_{10}(j_k)}\right|$ decreases correspondingly. When $U > 0.5$ V, $\frac{dU}{d\log_{10}(j_k)}$ reaches the typical value of Tafel slope, −117 mV/decade, and keeps as a constant even till $U = 1.0$ V. This high Tafel slope at high U region also agrees with experimental results on Pt (1 0 0) surface [27,36]. However, the extremely high $\theta_{O_2^*}$ (~ 0.7 ML) in the medium potential region (0.6 V < U < 0.8 V) may be inaccurate for real Pt surface, because $E_{\mathrm{ads}}^{O_2^*}/h_{O_2^*}^0$ is not a simple linear function of $\theta_{O_2^*}$. As shown in Fig. 8 of Supplementary materials, the relatively low value of $\zeta_{O_2^*}^{O_2^*}$ (0.38 eV/ML) is only valid when $\theta_{O_2^*} \lesssim \frac{1}{2}$ ML, above which $E_{\mathrm{ads}}^{O_2^*}$ suddenly increases extremely fast with $\theta_{O_2^*}$ to more positive value, making the further adsorption of O_2 very difficult. For this reason, similar with the discussions for Pt (1 1 1) surface, better ORR kinetics and steady-state coverage of ORR intermediates could be expected if more accurate $E_{\mathrm{a}}^{\mathrm{DD}}(\theta_{j^*})$ [54] and $\mu_{i^*}(\theta_{j^*})$ relations are applied in our microkinetic model. These relations can be obtained by using larger and/or variant surface supercells in DFT calculations [21,55,56], higher order terms in $\mu_{i^*}(\theta_{j^*})$ functions [19], and even methods beyond mean-field approximations [20].

Beside the absolute ORR rates, we focus more on their relative ratios between Pt (1 1 1) and (1 0 0) surfaces. As shown in Fig. 4, although with significant differences in $h_{i^*}^0$ between two surfaces (−0.46 eV, +0.04 eV and −0.59 eV for O_2^*, O* and OH*, respectively), at steady states the maximum ratio of $j_{k(111)}/j_{k(100)}$ in the whole range of investigated U is only about 2.1. These small differences agree with experimental results where j_k on Pt (1 1 1) surface is only about twice of j_k on Pt (1 0 0) surface when $U = 0.9$ V [6]. So both the experiments and theoretical model have similar insensitivities of ORR rate to adsorption strengths on different catalytic surfaces.

To understand the origin of these low sensitivities, we plot ORR reaction pathway with step **AD** in Fig. 5a and b for Pt (1 1 1) and (1 0 0) surface, respectively. The reaction pathway at clean surface is also illustrated as dashed lines, which indicates that the free energy of the total system first goes down into a deep potential "well" because of low $\mu_{i^*}^0/h_{i^*}^0$ for certain intermediates (O* and OH*); there is also a large difference of $Q_{\mathrm{A}}^{\mathrm{RDS}}$ at zero coverage between two surfaces (0.23 eV when $U = 0.9$ V) because of the large differences in $h_{i^*}^0$. As the reaction goes on, the surface coverages of these stable intermediates rise since the steps to produce such intermediates (either forward or backward reactions) would have much higher rates than others, and their μ_{i^*} increase because of strong repulsive interactions as Eq. (14), which would reduce their accumulation rates in return. Finally, at steady states, the depths of "well" in reaction pathways are significantly reduced, so the reaction barriers and rates of most elementary steps become

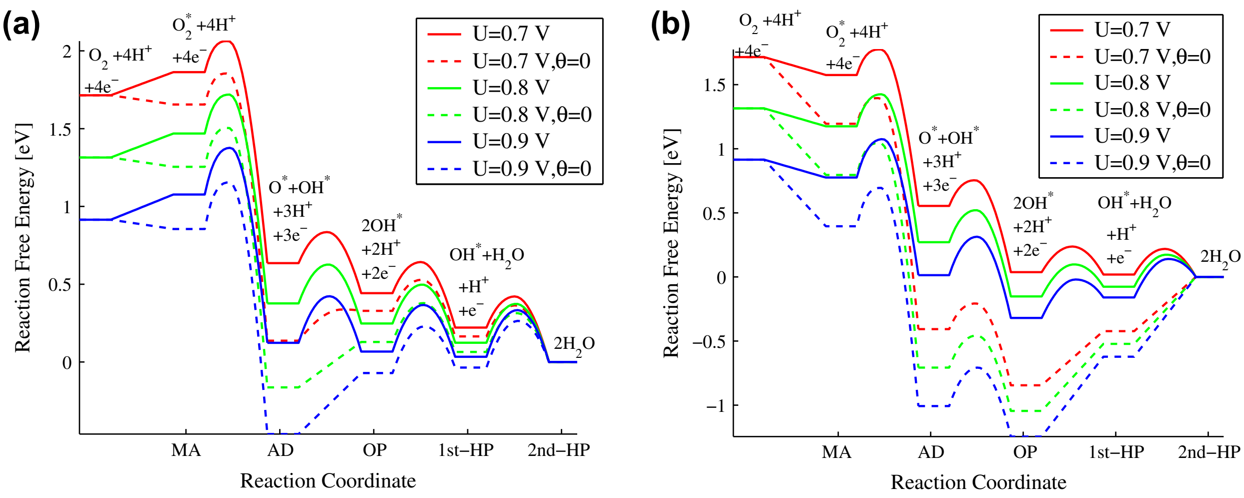

Fig. 5. Reaction path of ORR through O_2^* associated dissociation (**AD**) on Pt (1 1 1) (a) and Pt (1 0 0) (b) surface at different electrode potentials. The dashed curves are the reaction paths on clean surface with zero surface coverage ($\theta = 0$), and solid curves are paths at steady states.

comparable with each other and zero accumulation rate for each intermediate is achieved. We designate these changes in reaction rate ratios between different elementary steps as "self-regulation" effect. Because of this effect, activation barrier differences between Pt (1 1 1) and (1 0 0) surfaces become much smaller.

4. Sensitivity analyses

To quantitatively describe the above "self-regulation" effect, first-order sensitivity is calculated as Eq. (22). When there is only one RDS with maximum Q_A in the whole reaction network and the change in $h^0_{i^*}$ is the same as the change of Q_A^{RDS} [3,57], first-order sensitivity $\frac{d\log_{10}(j_k)}{dh^0_{i^*}} = \pm\frac{1}{k_BT}/\log(10) \approx \pm 16.8\ \mathrm{eV}^{-1}$ when $T = 300$ K; previous studies also showed that sensitivities would decrease when there are more than one RDS to compete for limited reaction sites or adsorbates ("entropic effect"), and the transition between these two sensitivity regions depends on reaction free energies [2]. Fig. 6a shows $\frac{d\log_{10}(j_k)}{dh^0_{i^*}}$ at steady states of ORR, where $h^0_{i^*}$ values of Pt (1 1 1) surface are applied but without enthalpic lateral interactions $\left(\zeta^{j^*}_{i^*} = 0\right)$. For $\frac{d\log_{10}(j_k)}{dh^0_{O^*}}$ and $\frac{d\log_{10}(j_k)}{dh^0_{OH^*}}$, when $U < 0.6V$, $\left|\frac{d\log_{10}(j_k)}{dh^0_{i^*}}\right| < +16.8\ \mathrm{eV}^{-1}$ because of the entropic effect and the limitation of maximum O_2 adsorption rate; when U increases (>0.6 V) and total reaction energy of ORR decreases correspondingly, $\frac{d\log_{10}(j_k)}{dh^0_{i^*}}$ becomes +16.8 eV^{-1} and $-16.8\ \mathrm{eV}^{-1}$ for O^* and OH^*, respectively, indicating step **OP** is the only RDS. On the other hand, as shown in Fig. 6b, with DFT-calculated $\zeta^{j^*}_{i^*}$ on Pt (1 1 1) surface, all $\frac{d\log_{10}(j_k)}{dh^0_{i^*}}$ become much smaller in the whole investigated potential region; they are even less than 1 eV^{-1} when $U < 0.85$ V. It means these lateral enthalpic interactions have much stronger effects to sensitivities than entropic effects. The magnitude of enthalpic effects depends on $\zeta^{j^*}_{i^*}$, which are usually very strong for large adsorbed atoms/molecules like oxygen and nitrogen atoms (1–2 eV/ML) [18,21], so it cannot be neglected.

Since all the sensitivities are calculated based on steady-state solutions of a specific surface, there would be significant changes in sensitivities when the surface is varied. To check this effect, we also calculate sensitivities on Pt (1 0 0) surface for both zero lateral interaction and lateral interaction cases as Pt (1 1 1) surface. As shown in Fig. 6c, if lateral interactions are not considered, all sensitivities are zero except $\frac{d\log_{10}(j_k)}{dh^0_{OH^*}}$, which goes to +16.8 eV^{-1} when

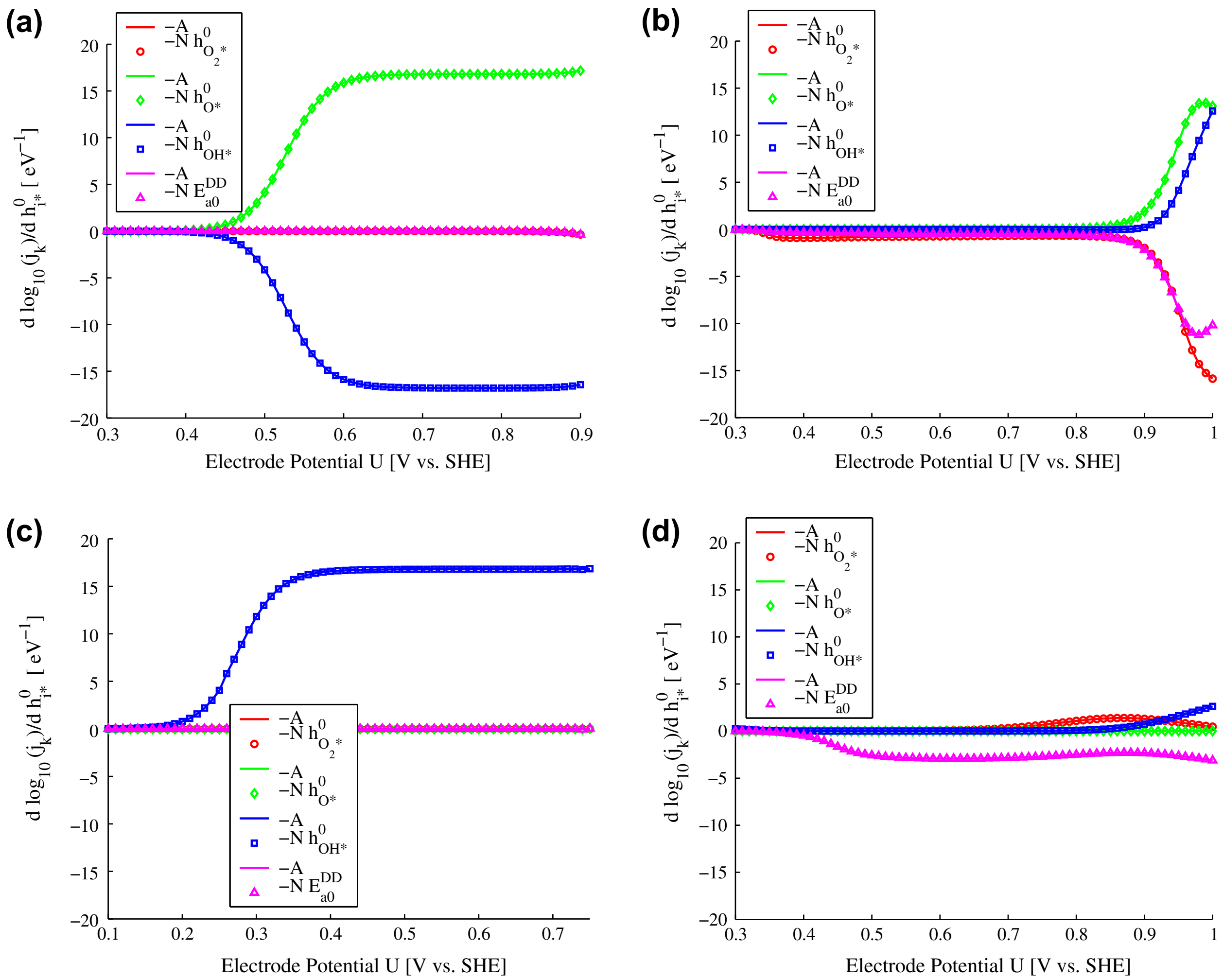

Fig. 6. Sensitivities of j_k to enthalpies of ORR intermediates (O_2^*, O^* and OH^*), $\frac{d\log_{10}(j_k)}{dh^0_{i^*}}$, and O_2^* dissociation barrier E^{DD}_{a0}, $\frac{d\log_{10}(j_k)}{dE^{DD}_{a0}}$. (a) and (c) Sensitivities with all $\zeta^{j^*}_{i^*} = 0$ for Pt (1 1 1) and (1 0 0) surface, respectively. (b) and (d) Sensitivities with values of $\zeta^{j^*}_{i^*}$ from Table 2 for Pt (1 1 1) and (1 0 0) surface, respectively. Here, "A" means results from analytical methods as Eq. (22), "N" means numerical results by calculating j_k variation when only one $h^0_{i^*}/E^{DD}_{a0}$ value changes by 10^{-6} eV. The consistence between analytical and numerical results supports the validity of Eq. (22).

$U > 0.4$ V. It means step **HP** is the only RDS because of the strong OH^* adsorption, which is also confirmed by total ORR paths on clean surface in Fig. 5b. Sensitivities with the consideration of lateral interactions are plotted in Fig. 6d, which shows very strong "self-regulation" effects since the maximum $\left|\frac{d\log_{10}(j_k)}{dh^0_{i^*}}\right|$ is less than 3.0 eV^{-1} during the whole investigated U region. In most of U region, $\frac{d\log_{10}(j_k)}{dE^{DD}_{a0}}$ has the maximum absolute value (-3 $eV^{-1} < \frac{d\log_{10}(j_k)}{dE^{DD}_{a0}} < -2$ eV^{-1}) so that lowering the barrier of step **DD** is the most critical factor to speed up overall ORR rate. $\frac{d\log_{10}(j_k)}{dh^0_{O_2^*}}$ and $\frac{d\log_{10}(j_k)}{dh^0_{OH^*}}$ are the two other none-zero sensitivities, both of which have positive values at high U region, suggesting the adsorptions of O_2^* and OH^* are too strong to achieve maximum ORR activity. In general, unlike the case of $\zeta^{j^*}_{i^*} = 0$ with only step **HP** as RDS, more than one elementary steps (**MA**, **DD**, **HP**, etc.) can affect ORR rate significantly with much lower sensitivities on Pt (100) surface.

Till now the sensitivity analyses are based on the assumption that each energetic parameter can be changed independently. However, for the real materials, the adsorption strengths of different atoms/molecules usually have the same variation tendencies with the changes of surface compositions and structures ("d-band center" theory [58,59]); meanwhile, on a specific surface there are always reaction intermediates with opposite sensitivities; as a result, these opposite sensitivities would compensate each other to reduce the overall effects of adsorption strength variations on reaction rates. In this context, as shown in Fig. 6b and d, we can classify these energetic parameters of ORR into two groups: the first group includes $h^0_{O_2^*}$ and E^{DD}_{a0}, which are related to ORR intermediates and/or transition states involved in the initial part of whole ORR reaction, and their increasing stabilities usually increase overall ORR rate (the only exception is $h^0_{O_2^*}$ for Pt (100) surface); the second group includes $h^0_{O^*}$ and $h^0_{OH^*}$, which are related to ORR intermediates and/or transition states involved in the final part of ORR reaction, and their increasing stabilities usually decrease overall ORR rate.

The above "compensation" effects can be further quantified when we consider the variations of all energetic parameters. For real catalysts, since these energetic parameters would change when the surface changes, a single first-order sensitivity cannot describe the variations of reaction rate with different surfaces. Fortunately, it was found that there may be approximately linear correlations between these energetic parameters [3,60,61]. By using these linear correlations, we can define net sensitivity as the following

$$\frac{\delta\log_{10}(j_k)}{\delta h^0_{O^*}} = \frac{d\log_{10}(j_k)}{dh^0_{O^*}} + \frac{dh^0_{O_2^*}}{dh^0_{O^*}}\cdot\frac{d\log_{10}(j_k)}{dh^0_{O_2^*}} + \frac{dh^0_{OH^*}}{dh^0_{O^*}}\cdot\frac{d\log_{10}(j_k)}{dh^0_{OH^*}} + \frac{dE^{DD}_{a0}}{dh^0_{O^*}}\cdot\frac{d\log_{10}(j_k)}{dE^{DD}_{a0}} \quad (23)$$

Different from first-order sensitivity defined in Eq. (19), net sensitivity is the summation of the first-order sensitivity for each energetic parameter $\left(\frac{d\log_{10}(j_k)}{dh^0_{i^*}}\right)$ multiplied by its correlation coefficient with the key parameter ($\frac{dh^0_{i^*}}{dh^0_{O^*}}$ here). It can quantify the variation of overall reaction rate with the adsorption strengths of different surfaces, which is described by the key energetic parameter ($h^0_{O^*}$ here). For the reaction intermediates of ORR investigated here, it was found that there is an approximate linear relation between the changes of $h^0_{OH^*}$ and those of $h^0_{O^*}$ on different metallic surfaces as $\delta h^0_{OH^*} \approx 0.50\delta h^0_{O^*}$ [61]; our DFT calculations also suggest an similar relation between $\delta h^0_{O_2^*}$ and $\delta h^0_{O^*}$ as $\delta h^0_{O_2^*} \approx 0.63\delta h^0_{O^*}$ on a series of (111) surface of FCC metals (details in Supplementary materials). We also assume $\delta E^{DD}_{a0} \approx \frac{1}{2}(2\cdot\delta h^0_{O^*} - \delta h^0_{O_2^*}) \approx 0.69\delta h^0_{O^*}$. Thus, we plot $\frac{\delta\log_{10}(j_k)}{\delta h^0_{O^*}}$ on Pt (111) surface in Fig. 7a, where $\frac{\delta\log_{10}(j_k)}{\delta h^0_{O^*}} \approx \frac{d\log_{10}(j_k)}{dh^0_{O^*}} + 0.63\cdot\frac{d\log_{10}(j_k)}{dh^0_{O_2^*}} + 0.50\cdot\frac{d\log_{10}(j_k)}{dh^0_{OH^*}} + 0.69\frac{d\log_{10}(j_k)}{dE^{DD}_{a0}}$. It shows that in the intermediate U region, ORR activity increases as adsorption strengths of Pt (111) surface increase; on the other hand, weaker adsorption strengths would induce better ORR activity in very high U region (>0.95 V here, and this transition potential depends on the accuracy of energetic parameters used in the microkinetic model). Compared with $\frac{d\log_{10}(j_k)}{dh^0_{i^*}}$ which may go to high limiting values, such as >10 eV^{-1} as shown in Fig. 6b, $\frac{\delta\log_{10}(j_k)}{\delta h^0_{O^*}}$ is much smaller (<3 eV^{-1}) in the whole investigated U range. Our analysis above quantitatively explains why on Pt alloys, which have similar adsorption strength

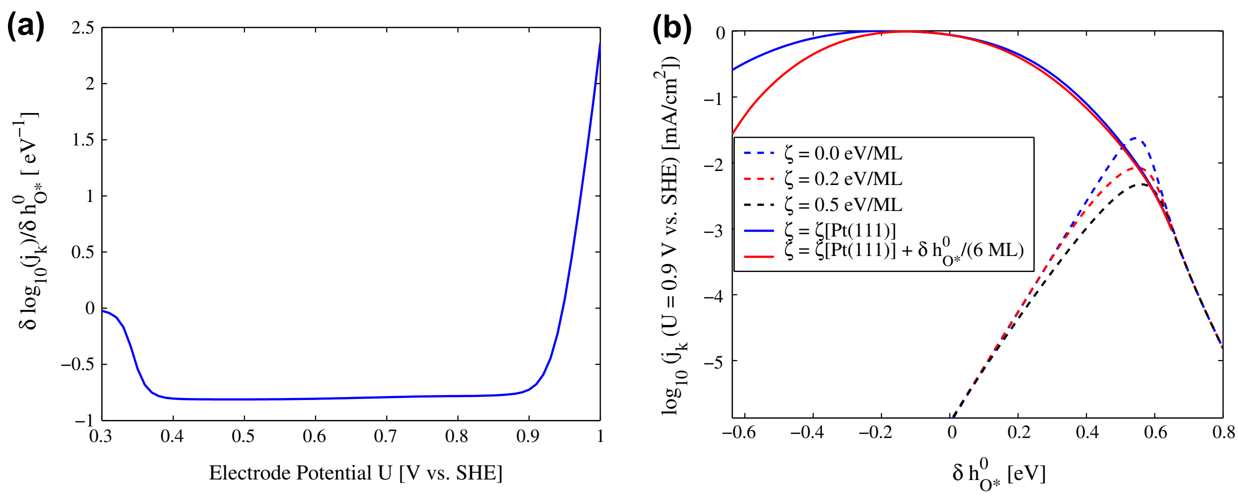

Fig. 7. (a) Net sensitivity defined in Eq. (23) for Pt (111) surface. (b) Volcano plots of ORR ($\log_{10}(j_k(U = 0.9$ V vs. SHE) (mA/cm^2)) vs. $\delta h^0_{O^*}$) with different $\zeta^{j^*}_{i^*}$ parameters. Here, $\delta h^0_{O^*} = 0$ corresponds to adsorption strength on Pt (111) surface. All other $h^0_{i^*}/E^{DD}_{a0}$ also change with $h^0_{O^*}$ as $\frac{dh^0_{O_2^*}}{dh^0_{O^*}} = 0.63$, $\frac{dh^0_{OH^*}}{dh^0_{O^*}} = 0.5$ and $\frac{dE^{DD}_{a0}}{dh^0_{O^*}} = 0.69$. All $\zeta^{j^*}_{i^*}$ are equal to 0.0, 0.2, and 0.5 eV/ML (dashed curves), respectively, or based on values on Pt (111) surface from Table 2 (solid curves). For the latter cases, when $h^0_{O^*}$ changes, all $\zeta^{j^*}_{i^*}$ are either fixed or change with $h^0_{O^*}$ as $\delta\zeta^{j^*}_{i^*} = \frac{1}{6ML}\delta h^0_{O^*}$, which corresponds to the more realistic situations where the lateral repulsions decrease as adsorption strengths increase [18].

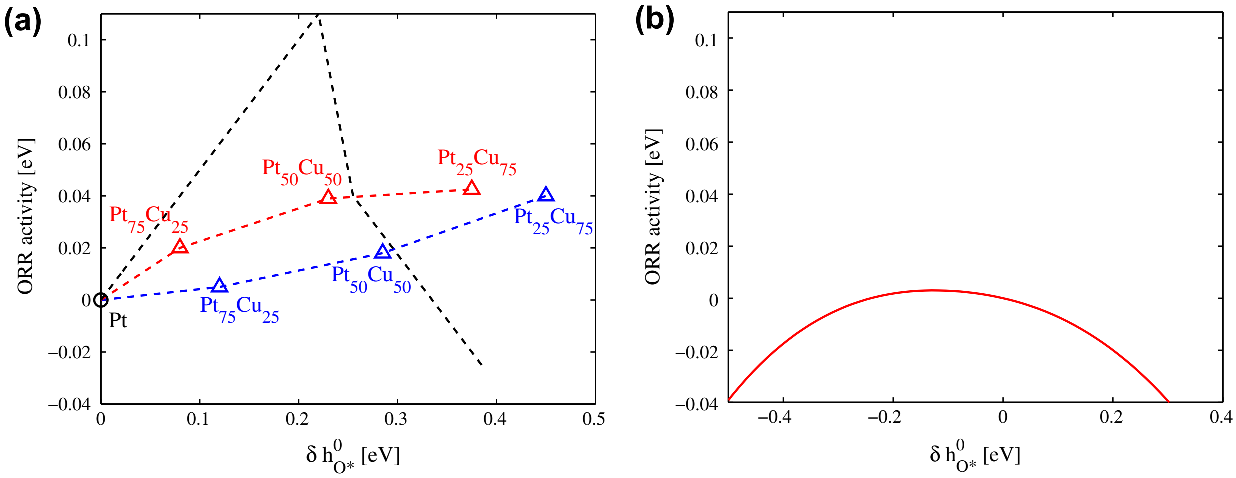

Fig. 8. (a) The experimental ORR activity in units of $k_BT \cdot \ln(j_{k,\mathrm{alloy}}/j_{k,\mathrm{Pt}})$ at U = 0.9 V of two families of dealloyed Pt–Cu bimetallic core–shell nanoparticles plotted as a function of $\delta h^0_{O^*}$ resulting from strain in the pure Pt particle shell (red and blue triangles denote dealloyed Pt–Cu precursors prepared at annealing temperatures of 800 °C and 950 °C, respectively) [9]. In their original volcano plot, the strain magnitude on Pt surface was used as x-axis, which we change to $\delta h^0_{O^*}$ based on DFT calculations (details in Supplementary materials). The black dashed line is the DFT-predicted, volcano-shaped trend of the ORR activity for a Pt (1 1 1) single-crystal slab under isotropic strain [4,9]. (b) The relation between isotropic surface strain and variation of adsorption strength $\delta h^0_{O^*}$ on Pt (1 1 1) surface obtained from DFT calculations. (c) Volcano plot of ORR activity in units of $k_BT \cdot \ln(j_k/j_{k,\mathrm{Pt}(111)})$ at U = 0.9 V from our microkinetic model, where all $\zeta^{j^*}_{i^*}$ change with $h^0_{O^*}$ as $\delta\zeta^{j^*}_{i^*} = \frac{1}{6\mathrm{ML}}\delta h^0_{O^*}$ as Fig. 7b.

and surface structures as pure Pt so that their sensitivities should also be close to each other, the changes in specific activity are so small [7,51].

Because volcano plot is the integral effect of $\frac{\delta \log_{10}(j_k)}{\delta h^0_{O^*}}$, the small net sensitivity indicates that the volcano could be very flat. Fig. 7b shows the volcano plot of our ORR model, $\log_{10}(j_k(U = 0.9\mathrm{V\ vs.\ SHE}))\left(h^0_{O^*}\right)$, based on results on Pt (1 1 1). Here, all the adsorption energies/enthalpies ($E^{i^*}_{\mathrm{ads0}}/h^0_{i^*}$) are the same as Pt (1 1 1), but different lateral interaction values ($\zeta^{j^*}_{i^*}$) are applied in order to investigate the effects of both entropic and enthalpic interactions to volcano plot. Under purely entropic interaction $\left(\zeta^{j^*}_{i^*} = 0\right)$, the top of volcano is already flattened [2,13]. As each $\zeta^{j^*}_{i^*}$ increases equally from zero to high value (0.5 eV/ML), the flatness of the volcano top also increases and the maximum activity decreases because of enthalpic effect.

When DFT-calculated $\zeta^{j^*}_{i^*}$ values are applied, there are two major changes shown as solid lines in Fig. 7b. First, the optimal adsorption energy and corresponding maximum activity change significantly compared with the cases of equal $\zeta^{j^*}_{i^*}$. It results from the differences in $\zeta^{j^*}_{i^*}$ parameters (varying from 0.1 to 2.1 eV/ML shown in Table 2), which would change the relative stabilities of ORR intermediates and corresponding reaction pathways at steady states as shown in Fig. 5. Second, because of certain strong $\zeta^{j^*}_{i^*}$ values, the flat adsorption energy range $h^0_{O^*}$ increases significantly and there is large $h^0_{O^*}$ range where activity is close to the possible maximum activity, which explains why so many types of Pt alloys have similar specific activities. Far away from the top, "volcanoes" transform back to straight lines, because j_k is limited by $\theta_{O_2^*}$ and θ_* when adsorption becomes very weak and strong, respectively, and $\theta_{O_2^*}$ and θ_* behave as Langmuir isotherms in the Boltzmann distribution limit [1]. At the extreme of weak adsorption (right side of volcano plot), all θ_{i^*} are small and there is almost no enthalpic effect from $\zeta^{j^*}_{i^*}$; at the extreme of strong adsorption (the left side), θ_* is proportional to $\exp\left(-\frac{h_{i^*}}{k_BT}\right) = \exp\left(-\frac{h^0_{i^*} + \sum_j \zeta^{j^*}_{i^*}\theta_{j^*}}{k_BT}\right)$ and certain θ_{j^*} reaches high value close to 1 ML; thus, the flattened adsorption energy range $h^0_{O^*}$ would scale linearly with ζ, a characteristic lateral interaction energy, as illustrated in Fig. 1.

Finally, we show a comparison of ORR volcano plots from both our model and experimental measurements. As shown in Fig. 8a, Strasser et al. tuned the adsorption strengths of Pt surface shell by compressive strain from Pt–Cu alloys in the core of core–shell structured nanoparticles [9], and ORR activity is described by the change of effective activation energy of ORR current density (Q_A in $j_k \equiv j^0_k \cdot \exp\left(-\frac{Q_A}{k_BT}\right)$) relative to that of pure Pt nanoparticles. This experimental volcano plot indicates that ORR activity continuously increases as the compressive strain increases $\delta h^0_{O^*}$ by ~0.4 eV, but the corresponding variation of Q_A is only ~0.04 eV. Thus, on Pt surfaces ~0.4 eV of $\delta h^0_{O^*}/\delta E^{O^*}_{\mathrm{ads}}$ only results into ~0.04 eV change in the effective ORR activation energy. This sensitivity is much lower than previous thermal-kinetic models, such as $\delta Q_A \approx \pm\delta E_{\mathrm{ADS}}$, corresponding to the black dashed lines in Fig. 8a [3,4]. On the other hand, we re-plot the volcano from our microkinetic model by using the change of effective ORR activation energy in Fig. 8b. It confirms that 0.3–0.4 eV of $\delta h^0_{O^*}$ from the maximum point of the volcano only results in change of activation energy of ~0.04 eV.

However, there is a mismatch of optimal $\delta h^0_{O^*}$ to reach the maximum activity (volcano peak location) between our result and the experimental volcano plots [9,62]. We believe it arises from several factors. First, there are inaccuracies of the enthalpies of surface adsorbates, which could be improved by more accurate DFT energy functionals and pseudopotentials, such as revised PBE functionals [63], and/or thermodynamic corrections of free energies at electrochemical interface [64]. Second, our volcano plot is based on several approximate linear relations between $\delta h^0_{O^*}$ and all other energetic parameters as Eq. (23). These linear relations are generally correct on a large energy scale (several eV) but with local fluctuations [61], which may also bring errors to the optimal $\delta h^0_{O^*}$. Third and most importantly, our simplified ORR model neglects the effect of H_2O, except adding a constant solvation energy correction to the enthalpy of OH* (details in Supplementary materials). Although isolated H_2O molecule can be easily desorbed from Pt surface due to weak adsorption, there are strong interactions between OH* and H_2O^* that depend on their molecular orientations (OH bond of OH*/H_2O^* should point to O atom of nearby H_2O^*/OH* to form strong hydrogen bonding), which result in stable and ordered structure of co-adsorption of OH* and H_2O^* on Pt (1 1 1) surface [34,65]. Based on the same mechanism, there could be another ordered and stable OH^*/H_2O^* co-adsorption structure on Pt (100) surface with different free energies. Thus, the description of free energies of reaction intermediates as linear functions of θ_{i^*} like Eq. (18) is inaccurate for real ORR in aqueous environment, so it does not provide the volcano peak location quantitatively. We need a better surface reaction model beyond the mean-field approximation to study the free energy of reaction intermediates as function of their coverage and adsorbed H_2O. Nevertheless, because there are strong interactions between other ORR intermediates, which can still significantly decrease the differences in free-energy extrema by the "self-regulation" mechanism described in Section 3, the general conclusion of low sensitivity of ORR resulting from lateral interactions based on our sensitivity analysis is still valid.

5. Conclusions

ORR on the cathode of PEM fuel cells is a typical electrocatalytic reaction with complicated reaction mechanisms. We propose a mean-field ORR microkinetic model based on first-principles methods, which considers both the competitions of surface sites/adsorbates (*entropic interactions*) and the lateral attraction/repulsion (*enthalpic interactions*) between different ORR intermediates adsorbed on Pt surfaces. Its most important outcome is that different surfaces, such as Pt (111) vs. Pt (100), with significantly different adsorption strengths for ORR intermediates only induce small variations in total ORR rates at steady states [7], validating the experimentally observed low sensitivity of ORR catalytic activity to adsorption strengths on catalytic materials like Pt alloys [8,51].

To quantitatively analyze the mechanism of insensitivities, we calculate the sensitivities of ORR rate to the change of stability of each individual ORR intermediate [22–24]. First, it shows that the typical rate-determining step (RDS) with maximum activation free energy is not rigorously defined for this surface reaction with limited reaction sites [12,13], since all the elementary steps usually have similar rates under the steady-state constraints. Second, it suggests that the insensitivities result from two aspects: a "self-regulation" feedback mechanism, which results mostly from *enthalpic interactions* other than *entropic interactions*, and a "compensation" mechanism, which means the sensitivities of intermediates involved in the initial steps and those in final steps usually have opposite signs. Under the influence of these two effects, the net sensitivity of ORR rate to the adsorption strength on surface is very small for catalysts of industrial interest, which are already near the top of the volcano. It means the volcano plot of our ORR model, which is the integration effect of the net sensitivity, has very flat top and the flatness increases with the characteristic lateral interaction energy. In addition, the finite interactions between various reaction intermediates may also shift the optimal adsorption energy and the corresponding maximum activity in the volcano plots, as shown in Figs. 7b and 1.

Our ORR model is based on the mean-field approximation and only considers three reaction intermediates (O_2^*, O^*, and OH^*). In real ORR under aqueous environment, there are orientation-dependent strong interactions between OH^* and adsorbed H_2O^* that cannot be described by the mean-field approximation [34,65]. As a result, our model does not provide quantitatively accurate optimal adsorption energy compared with the experimental volcano plots [9,62]. However, since there are strong interactions between different types of ORR intermediates, neglecting of interactions between OH^* and H_2O^* would not significantly affect the agreement on the scale of sensitivity between experiments and our model. In general, our model and analyses provide a systematic method to quantitatively investigate the sensitivities of surface reactions that involve only relatively simple atomic/molecular adsorbates (like O^*/OH^*) so that mean-field approximation is reasonable. The main qualitative features (a) greatly reduced sensitivity, (b) flattened volcano top ($\propto$ enthalpic ζ or entropic k_BT), and (c) shifted volcano center due to lateral interactions are reflected in the particular quantitative instances of this paper, but they should also be generic principles that underlie a wide range of catalysis phenomena. In short, "it is flat and crowded at the top".

Acknowledgments

We acknowledge support by AFOSR FA9550-08-1-0325 and thank Yoshiya Fujiwara for helpful discussions.

Appendix A. Supplementary material

Supplementary data associated with this article can be found, in the online version, at http://dx.doi.org/10.1016/j.jcat.2012.07.019.

References

[1] G.A. Somorjai, Chemistry in Two Dimensions: Surfaces, Cornell University Press, 1981.
[2] T. Bligaard, J.K. Nørskov, S. Dahl, J. Matthiesen, C.H. Christensen, J. Sehested, J. Catal. 224 (2004) 206.
[3] J.K. Nørskov, J. Rossmeisl, A. Logadottir, L. Lindqvist, J.R. Kitchin, T. Bligaard, H. Jonsson, J. Phys. Chem. B 108 (2004) 17886.
[4] V. Stamenkovic, B.S. Mun, K.J.J. Mayrhofer, P.N. Ross, N.M. Markovic, J. Rossmeisl, J. Greeley, J.K. Nørskov, Angew. Chem. Int. Ed. 45 (2006) 2897.
[5] J. Zhang, M. Vukmirovic, K. Sasaki, A. Nilekar, M. Mavrikakis, R. Adzic, J. Am. Chem. Soc. 127 (2005) 12480.
[6] V.R. Stamenkovic, B. Fowler, B.S. Mun, G. Wang, P.N. Ross, C.A. Lucas, N.M. Markovic, Science 315 (2007) 493.
[7] V.R. Stamenkovic, B.S. Mun, M. Arenz, K.J.J. Mayrhofer, C.A. Lucas, G. Wang, P.N. Ross, N.M. Markovic, Nat. Mater. 6 (2007) 241.
[8] I.E.L. Stephens, A.S. Bondarenko, U. Gronbjerg, J. Rossmeisl, I. Chorkendorff, Energy Environ. Sci. 5 (2012) 6744.
[9] P. Strasser, S. Koh, T. Anniyev, J. Greeley, K. More, C. Yu, Z. Liu, S. Kaya, D. Nordlund, H. Ogasawara, et al., Nat. Chem. 2 (2010) 454.
[10] R. Parsons, Trans. Faraday Soc. 54 (1958) 1053.
[11] K. Reuter, D. Frenkel, M. Scheffler, Phys. Rev. Lett. 93 (2004) 116105.
[12] J.X. Wang, J. Zhang, R.R. Adzic, J. Phys. Chem. A 111 (2007) 12702.
[13] J. Rossmeisl, G.S. Karlberg, T. Jaramillo, J.K. Nørskov, Faraday Discuss. 140 (2008) 337.
[14] J. Cheng, P. Hu, J. Am. Chem. Soc. 130 (2008) 10868.
[15] K. Honkala, A. Hellman, I. Remediakis, A. Logadottir, A. Carlsson, S. Dahl, C. Christensen, J. Nørskov, Science 307 (2005) 555.
[16] G.S. Karlberg, T.F. Jaramillo, E. Skulason, J. Rossmeisl, T. Bligaard, J.K. Nørskov, Phys. Rev. Lett. 99 (2007) 126101.
[17] H. Meskine, S. Matera, M. Scheffler, K. Reuter, H. Metiu, Surf. Sci. 603 (2009) 1724.
[18] D.A. Hansgen, D.G. Vlachos, J.G. Chen, Nat. Chem. 2 (2010) 484.
[19] L.C. Grabow, B. Hvolbæk, J.K. Nørskov, Topic Catal. 53 (2010) 298.
[20] C. Wu, D.J. Schmidt, C. Wolverton, W.F. Schneider, J. Catal. 286 (2012) 88.
[21] R.B. Getman, Y. Xu, W.F. Schneider, J. Phys. Chem. C 112 (2008) 9559.
[22] S. Kozuch, S. Shaik, J. Am. Chem. Soc. 128 (2006) 3355.
[23] S. Kozuch, S. Shaik, J. Phys. Chem. A 112 (2008) 6032.
[24] C. Stegelmann, A. Andreasen, C.T. Campbell, J. Am. Chem. Soc. 131 (2009) 8077.
[25] L. Qi, X.F. Qian, J. Li, Phys. Rev. Lett. 101 (2008) 146101.
[26] R.I. Cukier, D.G. Nocera, Annu. Rev. Phys. Chem. 49 (1998) 337.
[27] N.M. Markovic, H.A. Gasteiger, P.N. Ross, J. Phys. Chem. 99 (1995) 3411.
[28] L. Qi, J. Yu, J. Li, J. Chem. Phys. 125 (2006) 054701.
[29] M.P. Hyman, J.W. Medlin, J. Phys. Chem. B 110 (2006) 15338.
[30] M. Eigen, Angew. Chem. Int. Edn. Engl. 3 (1964) 1.
[31] G. Zundel, H. Metzger, Z. Physik. Chem. (N.F.) 58 (1968) 225.
[32] D. Marx, M.E. Tuckerman, J. Hutter, M. Parrinello, Nature 397 (1999) 601.
[33] J.O. Bockris, A.K.N. Reddy, M. Gamboa-Aldeco, Modern Electrochemistry 1: Ionics, second ed., Springer, 1998.
[34] J. Rossmeisl, J.K. Nørskov, C.D. Taylor, M.J. Janik, M. Neurock, J. Phys. Chem. B 110 (2006) 21833.
[35] B.N. Grgur, N.M. Markovic, P.N. Ross, J. Phys. Chem. B 101 (1997) 5405.
[36] N.M. Markovic, H.A. Gasteiger, P.N. Ross, J. Electrochem. Soc. 144 (1997) 1591.
[37] R.A. Sidik, A.B. Anderson, J. Electroanal. Chem. 528 (2002) 69.
[38] M. Aryanpour, V. Rai, H. Pitsch, J. Electrochem. Soc. 153 (2006) E52.
[39] M.J. Janik, C.D. Taylor, M. Neurock, J. Electrochem. Soc. 156 (2009) B126.
[40] A. Eichler, J. Hafner, Phys. Rev. Lett. 79 (1997) 4481.
[41] Z. Wang, C. Wang, K. Chen, J. Power Sources 94 (2001) 40.
[42] A. Rowe, X. Li, J. Power Sources 102 (2001) 82.
[43] S. Um, C. Wang, J. Power Sources 125 (2004) 40.
[44] R. Baetzold, G. Somorjai, J. Catal. 45 (1976) 94.
[45] M. Williams, H. Kunz, J. Fenton, J. Electrochem. Soc. 151 (2004) A1617.

[46] G. Kresse, J. Hafner, Phys. Rev. B 47 (1993) 558.
[47] G. Kresse, J. Furthmüller, Phys. Rev. B 54 (1996) 11169.
[48] P.E. Blöchl, Phys. Rev. B 50 (1994) 17953.
[49] J.P. Perdew, K. Burke, M. Ernzerhof, Phys. Rev. Lett. 77 (1996) 3865.
[50] U.A. Paulus, A. Wokaun, G.G. Scherer, T.J. Schmidt, V. Stamenkovic, V. Radmilovic, N.M. Markovic, P.N. Ross, J. Phys. Chem. B 106 (2002) 4181.
[51] H.A. Gasteiger, S.S. Kocha, B. Sompalli, F.T. Wagner, Appl. Catal. B – Environ. 56 (2005) 9.
[52] C.A. Wraight, Biochim. Biophys. Acta – Bioener. 1757 (2006) 886.
[53] W. Schmickler, Interfacial Electrochemistry, Oxford University Express, 1996.
[54] R.B. Getman, W.F. Schneider, A.D. Smeltz, W.N. Delgass, F.H. Ribeiro, Phys. Rev. Lett. 102 (2009) 076101.
[55] X.-G. Wang, G.B. Fisher, Phys. Rev. Lett. 99 (2007) 066101.
[56] S.D. Miller, J.R. Kitchin, Surf. Sci. 603 (2009) 794.
[57] D. Truhlar, B. Garrett, S. Klippenstein, J. Phys. Chem. 100 (1996) 12771.
[58] B. Hammer, J.K. Nørskov, Surf. Sci. 343 (1995) 211.
[59] B. Hammer, J.K. Nørskov, Adv. Catal. 45 (2000) 71–129.
[60] J.K. Nørskov, T. Bligaard, A. Logadottir, S. Bahn, L.B. Hansen, M. Bollinger, H. Bengaard, B. Hammer, Z. Sljivancanin, M. Mavrikakis, et al., J. Catal. 209 (2002) 275.
[61] J. Rossmeisl, A. Logadottir, J. Nørskov, Chem. Phys. 319 (2005) 178.
[62] I.E.L. Stephens, A.S. Bondarenko, F.J. Perez-Alonso, F. Calle-Vallejo, L. Bech, T.P. Johansson, A.K. Jepsen, R. Frydendal, B.P. Knudsen, J. Rossmeisl, et al., J. Am. Chem. Soc. 133 (2011) 5485.
[63] B. Hammer, L.B. Hansen, J.K. Nørskov, Phys. Rev. B 59 (1999) 7413.
[64] C.D. Taylor, S.A. Wasileski, J.S. Filhol, M. Neurock, Phys. Rev. B 73 (2006) 165402.
[65] A.S. Bondarenko, I.E.L. Stephens, H.A. Hansen, F.J. Perez-Alonso, V. Tripkovic, T.P. Johansson, J. Rossmeisl, J.K. Norskov, I. Chorkendorff, Langmuir 27 (2011) 2058.